Molecular Cell

Article

$GABA_A$ receptor π forms channels that stimulate ERK through a G-protein-dependent pathway

Graphical abstract

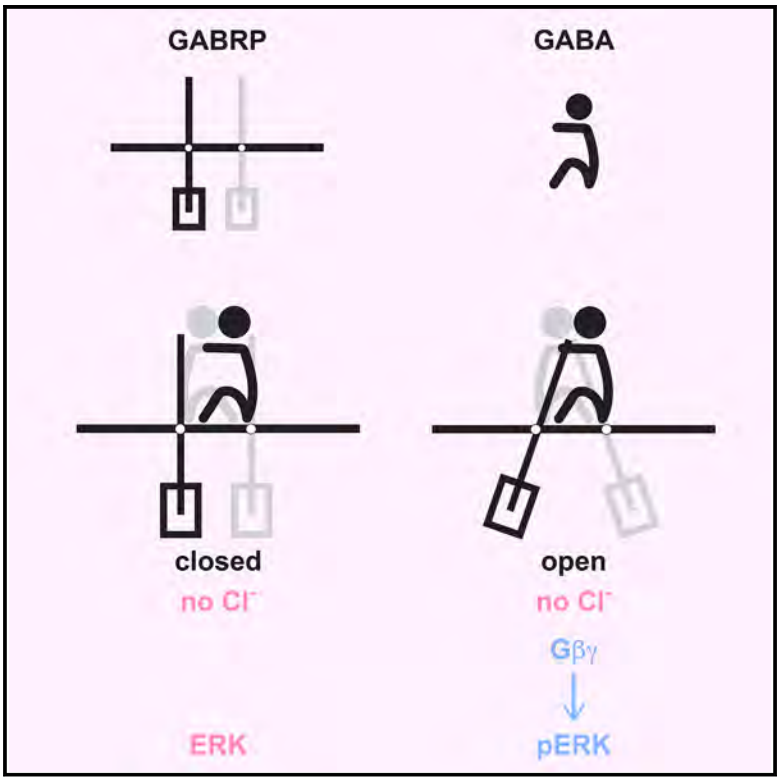

Highlights

- Homopentamers of GABAA receptor π (GABRP) subunits form GABA-regulated channels
- Cryo-EM of GABRP reveals a clear GABA-induced transition controlling channel pore size
- Despite its ion channel structure, GABRP selectively induces a metabotropic-like response
- An antibody targeting GABRP or Gβγ/PI3Kγ inhibition blocks GABA-induced ERK signaling

Authors

Yueyue Wang, Yalan Zhang, Wenxue Li, ..., Leonard K. Kaczmarek, Lajos Pusztai, Daryl E. Klein

Correspondence

daryl.klein@yale.edu

In brief

$GABA_A$ receptor π (GABRP) can form homopentameric channel-like structures, similar to the more common heteromeric type-A GABA receptor channels. However, GABRP activation by GABA uniquely induces a G-protein-signaling pathway rather than allowing chloride passage. Selective inhibition of GABRP signaling may hold therapeutic promise for GABRP-associated cancers.

Wang et al., 2025, Molecular Cell *85*, 166–176
January 2, 2025
https://doi.org/10.1016/j.molcel.2024.11.016

CellPress

CellPress

Molecular Cell

Article

$GABA_A$ receptor π forms channels that stimulate ERK through a G-protein-dependent pathway

Yueyue Wang,[1,2] Yalan Zhang,[3] Wenxue Li,[1,3] Barbora Salovska,[1,3] Jianan Zhang,[1,3] Tongqing Li,[1,3] Hengyi Li,[1,3] Yansheng Liu,[1,3,4] Leonard K. Kaczmarek,[3] Lajos Pusztai,[2] and Daryl E. Klein[1,3,5,*]

[1]Yale Cancer Biology Institute, Yale University, West Haven, CT 06516, USA
[2]Breast Medical Oncology, Yale Cancer Center, Yale University School of Medicine, New Haven, CT 06520, USA
[3]Department of Pharmacology, Yale University School of Medicine, New Haven, CT 06520, USA
[4]Department of Biomedical Informatics & Data Science, Yale University School of Medicine, New Haven, CT 06510, USA
[5]Lead contact
*Correspondence: daryl.klein@yale.edu
https://doi.org/10.1016/j.molcel.2024.11.016

SUMMARY

The rare γ-aminobutyric acid type-A receptor ($GABA_AR$) subunit π (GABRP) is highly expressed in certain cancers, where it stimulates growth through extracellular-regulated kinase (ERK) signaling by an uncharacterized pathway. To elucidate GABRP's signaling mechanism, we determined cryoelectron microscopy (cryo-EM) structures of GABRP embedded in native nanodiscs, both in the presence and absence of GABA. Structurally, GABRP homopentamers closely resemble heteropentameric $GABA_AR$ anion channels, transitioning from a closed "resting" state to an open "active" state upon GABA binding. However, functional assays reveal that GABRP responds more like a type-B metabotropic receptor. At physiological concentrations of GABA, chloride flux is not detected. Rather, GABRP activates a G-protein-coupled pathway leading to ERK signaling. Ionotropic activity is only triggered at supraphysiological GABA concentrations, effectively decoupling it from GABRP's signaling functions. These findings provide a structural and functional blueprint for GABRP, opening new avenues for targeted inhibition of GABA growth signals in GABRP-positive cancers.

INTRODUCTION

γ-aminobutyric acid (GABA) is the main inhibitory neurotransmitter in the central nervous system (CNS) and modulates neuronal activity by binding to its receptors, known as GABA receptors.[1,2] There are two main types of GABA receptors: type-A ionotropic ($GABA_ARs$) and type-B metabotropic ($GABA_BRs$).[3] Ionotropic $GABA_ARs$ are heteropentameric, ligand-gated chloride channels, consisting of five subunits (out of a possible 19 different subunits) that surround a central ion-conducting pore.[1,4–7] Whereas, metabotropic $GABA_BRs$ are heterodimeric G-protein-coupled receptors (GPCRs) that signal through the pertussis-toxin-sensitive Gαi/o family.[8]

The $GABA_A$ receptor subunit π (GABRP) is one of the rarest subunits and, unlike other $GABA_AR$ subunits, is not abundant in the CNS.[9] Uniquely, GABRP is highly expressed in certain cancers, such as triple-negative breast cancer (TNBC),[10–12] pancreatic ductal adenocarcinoma,[13–15] and ovarian cancer,[16] where it activates mitogen-activated protein kinase (MAPK)/extracellular signal-related kinase (ERK).[12,13,16,17] ERK activation by a $GABA_AR$ anion channel is unusual, as a typical inward Cl^- current would lead to hyperpolarization of the cell.[18] Indeed, $GABA_AR$ agonists have been shown to inhibit growth of multiple neuronal tumors.[18] Thus, the GABRP-signaling pathway that leads to ERK activity remains uncharacterized.[12,13,16,17]

Despite its high expression in cancer, previous studies argue that GABRP is itself not capable of forming homopentameric channels and cannot bind directly to $GABA_AR$ agonists[9,19]—potentially suggesting an alternative function for this subunit. Contrary to this expectation, we show here that GABRP activity is directly regulated by GABA binding to GABRP homopentamers. Moreover, our structural studies of GABRP—performed in native lipids and (importantly) without the use of exogenous stabilizing molecules—reveal a clear GABA-induced "resting-to-active" channel transition that has not previously been visualized for a $GABA_AR$. However, chloride flux through GABRP channels is observed only at supraphysiological concentrations of GABA, whereas GABRP-induced ERK activation occurs at physiological concentrations. To help uncover GABRP's link to ERK activity, we used phosphoproteomic analysis to reveal signaling pathways regulated by GABA stimulation. Interestingly, and similar to metabotropic $GABA_BRs$, GABRP activation leads to Gαi/o signaling. These results demonstrate that GABRP channels induce ERK activity through G-protein signaling (without conducting ions), blurring the established

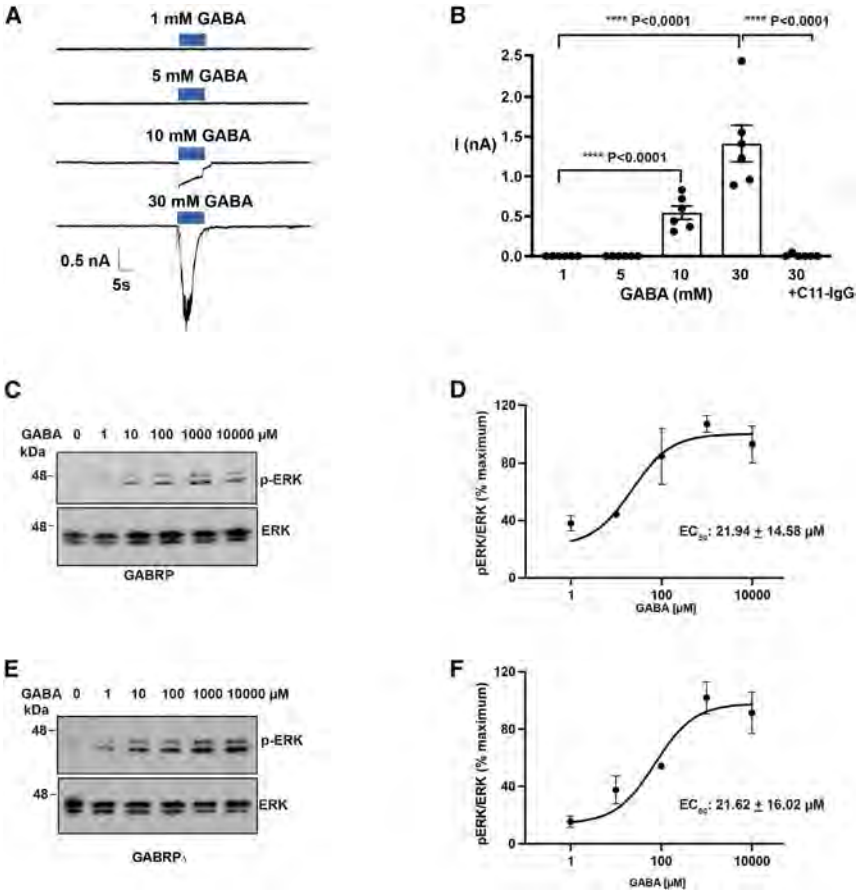

Figure 1. GABRP is responsive to GABA stimulation

(A) Representative whole-cell recording traces showing the response of GABRP-expressing cells to different GABA concentrations.

(B) Dot plot of evoked peak currents. Significant *p* values reported from one-way ANOVA ($n = 6$).

(C) Representative western blot of ERK phosphorylation as a function of GABA concentration for HEK293 cells stably expressing GABRP.

(D) A plot of the pERK/ERK ratio in GABRP cells as a function of GABA concentration for 3 independent biological repeats, plotting mean ± SD ($n = 3$). The data were fit to a dose-response stimulation curve (GraphPad Prism 9.0).

(E) Representative western blot of ERK phosphorylation as a function of GABA concentration for HEK293 cells stably expressing $GABRP_{\Delta}$.

(F) A plot of the pERK/ERK ratio in $GABRP_{\Delta}$ cells as a function of GABA concentration for 3 independent biological repeats, plotting mean ± SD ($n = 3$). Data were fit to a dose-response stimulation curve (GraphPad Prism 9.0).

functional dichotomy between $GABA_A$ and $GABA_B$ receptor subtypes.

RESULTS

GABA regulates GABRP activity

To examine the potential channel and signaling activity of GABRP, we overexpressed the receptor in HEK293 cells, which do not endogenously express appreciable levels of $GABA_AR$ subunits.[20] We initially subjected cells stably expressing GABRP at low levels (Figures S1A and S1B) to whole-cell patch-clamp recording to measure Cl^- conductance. Unexpectedly, and contrary to prior reports,[9,19] we found that application of GABA (as described in STAR Methods) induced an inward current in cells stably expressing GABRP held at a resting potential of −60 mV, whereas parental HEK293 cells showed no response to GABA (Figures S1C and S1D). To enhance GABRP expression, we used a strategy common for other $GABA_ARs$: removing the intracellular linker between the third and fourth predicted transmembrane (TM) domain (herein, $GABRP_{\Delta}$). This deletion has been used extensively in structural studies of $GABA_ARs$, as it increases receptor expression while retaining channel function.[21–24] Consistent with this, stable cells expressing $GABRP_{\Delta}$ showed significantly higher expression levels of the receptor compared with full-length GABRP (Figure S1B). Patch-clamp whole-cell recordings of cells stably expressing $GABRP_{\Delta}$ showed a robust response to GABA, likely reflecting the increased receptor levels, with peak currents significantly greater than those for GABRP (Figures S1C and S1D). Thus, GABRP and $GABRP_{\Delta}$ are capable of functioning as GABA-regulated Cl^- channels.

Although our initial electrophysiology assays demonstrated that GABRP is capable of inducing chloride influx, these characterizations were qualitative and conducted at a single high concentration of GABA, applied at a distance from the cells. To obtain more precise and quantitative data, we tested multiple GABA concentrations directly on the cells (as described in STAR Methods). Using this technique, we found that GABA-induced chloride current was only observed at supraphysiologic concentrations (>10 mM) (Figures 1A and 1B), approximately 3 orders of magnitude greater than the EC50 for heteromeric $GABA_ARs$.[25] As with conventional multimeric $GABA_ARs$,[26] the response to maintained GABA application desensitized over a period of many seconds (t for 10 mM GABA, 5.9 ± 1.9 s, $n = 8$; for 30 mM GABA, 9.9 ± 4.6 s, $n = 6$, mean ± SEM). Thus, our findings are consistent with prior studies, including those that did not observe an electrophysiological response of GABRP to typical GABA concentrations. However, at high concentrations of GABA (30 mM) we observe robust inward current. Notably, this current can be inhibited by an antibody we developed toward the extracellular region of GABRP, C11-IgG (as described in STAR Methods), demonstrating specificity of the response.

Previous reports have linked GABRP expression to ERK activation in cancer cells.[17] We therefore also tested whether GABA could induce ERK signaling in cells that stably express GABRP or $GABRP_{\Delta}$. We observed robust ERK phosphorylation after addition of GABA to serum-starved cells that stably express GABRP (Figures 1C and 1D) or $GABRP_{\Delta}$ (Figures 1E and 1F) but not in

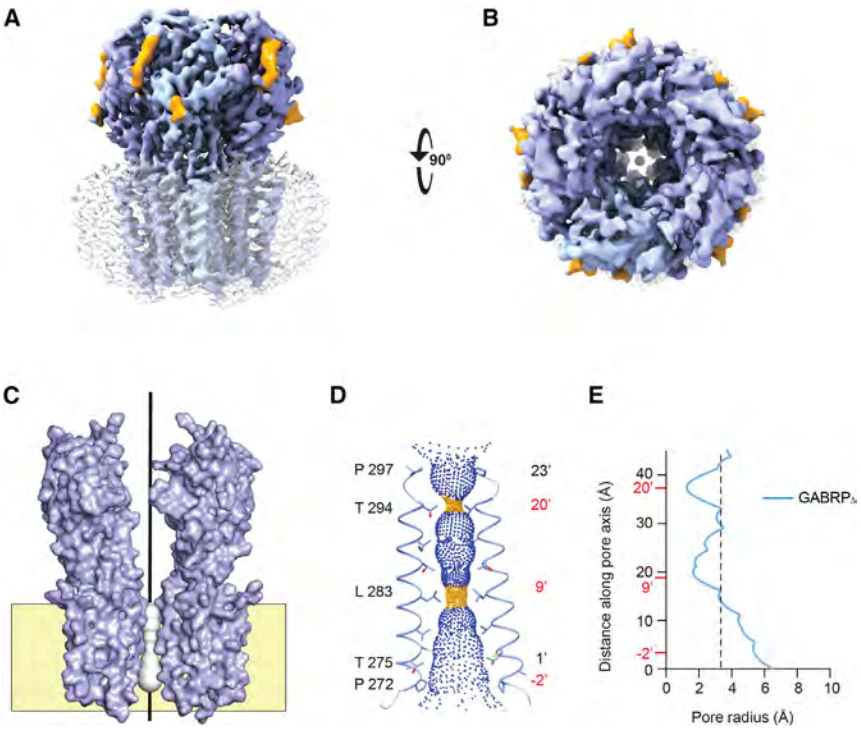

Figure 2. Cryo-EM structure of GABRP$_\Delta$ in a native nanodisc environment

(A and B) Side (A) and top (B) views of cryo-EM reconstruction map of homopentameric GABRP$_\Delta$ in native nanodiscs. A single subunit is colored in light blue for clarity. The nanodisc density is indicated with partially transparent white surface. Glycans are colored gold.

(C) View of the GABRP$_\Delta$ pentamer as in (A), but for simplicity only two opposing protomers of the complex are shown. The central channel is marked with a black rod and white spheres highlight the pore, calculated from MOLE*online*.[28] The yellow-shaded box approximates the region of the cell membrane.

(D) Ion permeation pathways for GABRP$_\Delta$, calculated by the program HOLE.[29] The second transmembrane (M2) helices of opposing protomers, with sidechains shown for pore-lining residues only. Small blue spheres represent the solvent accessible volume of the ion channel. Orange spheres are shown to highlight constrictions of the pore. Numbers -2′ to 23′ denote the residues of the pore-lining M2 helix. The intracellular, middle, and extracellular gate region numbers are colored red.

(E) HOLE plot of pore radius as a function of distance along the pore axis for GABRP$_\Delta$ in SMA. Dashed line at 3.32 Å representing the approximate radius of a hydrated chloride ion.

parental cells or in cells that express heteromeric (α, β, γ) GABA$_A$R subunits (Figure S1E). A dose-response analysis (Figures 1C–1F) shows nearly identical pERK responsiveness to GABA for GABRP or GABRP$_\Delta$, each with an EC$_{50}$ of ~21 μM, demonstrating that the intracellular loop removed in GABRP$_\Delta$ is not involved in this function of GABRP. Contrary to GABRP's ionotropic function, the EC$_{50}$ for ERK signaling is similar to the reported EC$_{50}$ for heteromeric GABA$_A$Rs[25]—demonstrating a similar physiologic sensitivity to GABA. Notably, when a supraphysiologic concentration of GABA is added to GABRP stable cells (at a concentration that induces chloride flux) the ERK response is diminished (Figure S1F)—consistent with the opposing roles of signaling and hyperpolarization. Together, these findings demonstrate that GABRP induces ERK signaling at physiologic GABA levels and can function as a GABA-responsive chloride channel at supraphysiologic GABA levels.

GABRP forms a homopentamer

Our finding that GABRP can function alone as a GABA-responsive chloride channel was surprising, given previous reports that it can neither form a homomeric channel nor bind GABA$_A$R agonists.[9,19] We therefore sought to determine the structural basis for GABRP activity to understand whether it differs mechanistically from its homologs. We used styrene maleic anhydride (SMA) native nanodiscs[27] to purify the receptor from HEK293 GnTI$^-$ cells, allowing us to isolate the protein in a native membrane context and without using detergents that could compromise its structure (Figures S2A–S2C).

Using cryoelectron microscopy (cryo-EM), we determined the structure of GABRP$_\Delta$ to a resolution of 3.07 Å (Figures S2D and S2E). The structure reveals that GABRP does indeed form a homopentamer, with an organization that is very similar to that seen in previously determined structures of GABA$_A$Rs and pentameric ligand-gated ion channels (pLGIC) (Figures 2A and 2B). The unliganded GABRP$_\Delta$ pentamer likely represents a non-conducting resting state. This state has not been observed in prior GABA$_A$R structures—likely due to effects imposed by detergent extraction and/or the impact of necessary stabilizing toxins, inhibitors, or antibodies,[21,22,24] which were not necessary for our studies in native nanodiscs. The resting-state pore of the unliganded GABRP$_\Delta$ channel is gated at two regions in which the radius of the channel falls to less than 2 Å (Figures 2C–2E). The activation gate is found at the middle of the channel pore in a position similar to other pLGICs in non-conducting states; L283 at 9′ (the 9th residue of the pore-lining TM segment 2; TM2) (Figures 2D and 2E; Figures S3A–S3D). GABRP$_\Delta$ also has a narrow pore radius at T294 (20′) that likely functions as an extracellular gate. Additionally, and consistent with unliganded GABRP$_\Delta$ representing a resting state (and not a desensitized state as in prior GABA$_A$R structures), the intracellular desensitization gate at P272 (-2′) is open, with a radius larger than 4 Å (Figures 2D and 2E; Figures S3A–S3D). Thus, the unliganded GABRP structure forms a previously unappreciated homopentamer and, to our knowledge, represents the structure of a resting-state (closed) GABA$_A$ receptor in a native membrane environment.

Structure of GABA-bound GABRP

We next determined the structure of GABRP$_\Delta$ in the presence of GABA, using the same purification protocol and strategy as for unliganded GABRP$_\Delta$ (Figures S2F and S2G). The resolution of the GABRP plus GABA structure (2.97 Å) is comparable with the unliganded receptor (Figures S2H and S2I). Overall, the

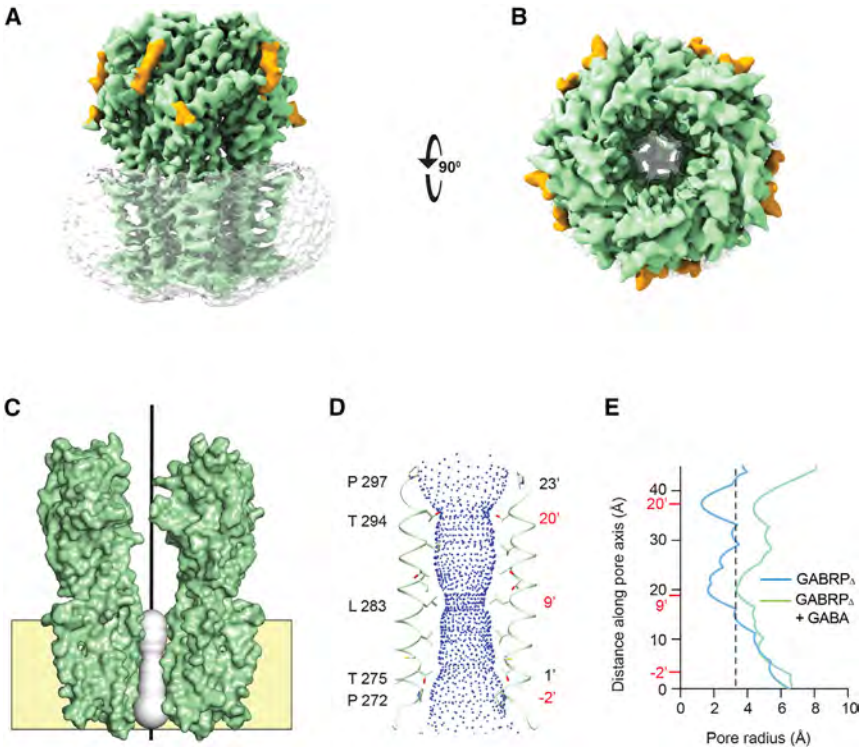

Figure 3. Cryo-EM structure of GABRP$_\Delta$ in native nanodiscs after GABA addition

(A and B) Side (A) and top (B) views of the cryo-EM reconstruction map of GABRP$_\Delta$ complexed with GABA in native nanodiscs. The nanodisc density is indicated with partially transparent white surface. Glycosylations are colored gold.

(C) View of the GABA-bound GABRP$_\Delta$ pentamer, as shown in Figure 2.

(D) Ion permeation pathway for GABRP$_\Delta$ after GABA addition, calculated by the program HOLE.[29]

(E) HOLE plot of the pore radius as a function of distance along the pore axis for GABRP$_\Delta$. Profiles in the absence (blue) and presence (green) of GABA are shown. Dashed line denotes the hydrated radius of chloride ions.

pore of the GABRP$_\Delta$ pentamer in the presence of GABA is larger than that in the unliganded structure (Figures 3A and 3B). The pore constrictions evident in the unliganded structure at 9′ L283 and 20′ T294 are enlarged to a radius of greater than 3.3 Å in the structure with GABA (Figures 3C–3E). Additionally, the charge of the pore is slightly positive, similar to that of other GABA$_A$Rs and anion channels, further supporting the ability of GABRP$_\Delta$ to function as an anion channel (Figure S4).

In the reconstruction there is clear density for GABA in each of the five ligand-binding pockets that sit between GABRP$_\Delta$ protomers (Figures 4A and 4B). GABA binding and coordination between protomers is very similar to other reported structures. GABRP maintains the key residues critical for GABA binding on both sides of the protomer, including R89 (site 1) and E179 (site 2) that hydrogen-bond to either side of GABA, as well as hydrophobic residues lining the pocket (Figure 4C). Having both ligand epitopes (one on each side of each protomer) is consistent with GABRP functioning as a homopentamer, as observed here. By comparison, the heteromeric GABA$_A$Rs subunits have only a single GABA-binding epitope per protomer, which is complemented by a different subunit to complete the binding pocket (Figures 4C and 4D).[21–24,30,31]

Nature of GABA-coupled channel opening

Despite a wealth of information from numerous recent GABA$_A$R structures,[21–24,30,31] a mechanistic understanding of how GABA regulates GABA$_A$R channel opening remains incomplete, and a clear transition from an unliganded closed "resting" state to a GABA-bound open "active" state has yet to be visualized.[33] Having obtained GABRP$_\Delta$ structures in both resting and active states in a native membrane environment—and without the need for stabilizing inhibitors or antibodies—allows us to examine the nature of GABA-induced channel activation more straightforwardly than has previously been possible. When the unliganded and GABA-bound GABRP$_\Delta$ structures are overlaid, a rotation of the extracellular domain (ECD) is apparent, about an axis parallel to the membrane (Figure 5A). The GABA-bound structure displays an ~5° rotation of the ECD compared with the resting state about this axis. Additionally, the extracellular ends of the TM domains are drawn away from the central pore by ~3 Å in a concerted way, in the same direction as the ECD rotation in the plane of the membrane (Figure 5B).

A defining feature of this superfamily of receptors is the presence of an ECD cystine (Cys) loop (GABRP disulfide pair C160–C174). This disulfide generates a "blade" of largely hydrophobic residues that is positioned in the middle of the 4 TM helices—thus linking the ECD to the TM region (Figures 5C and 5D). In GABRP, the Cys-loop blade is further connected to the ECD rotational axis via a continuation of the β-strand "shaft" that follows residue 174 (Figures 5C and 5D). GABA binds at the proximal end of this shaft, close to the GABRP$_\Delta$ ECD rotation axis, in a region that we term the "handle" (Figures 5C and 5D). Ligand binding is linked to the TMs of the receptor from this handle through to the shaft and Cys-loop blade.

In the ligand-bound structure, GABA links two adjacent protomers of the pentamer together—binding with a different set of interactions to each side of each ECD (Figure 4B). Ligand binding to "site 1" of each ECD (at R89) sits at a special position, passing through the ECD's axis of rotation (Figures 5D and 5E). By contrast, "site 2" (at the handle, including E179) is offset from the ECD's rotational axis (Figures 5C and 5F). Having one side of ligand bind on the rotation axis (site 1) ensures that this site will be maintained regardless of rotational state of the ECDs in the pentamer. Simultaneously, the other side of the ligand engages at a site that is offset from the rotation axis on an adjacent protomer (site 2), allowing GABA to control subunit rotation in the pentamer, stabilizing the rotated conformation of the active state. Of note, the ECD rotation axis passes directly through

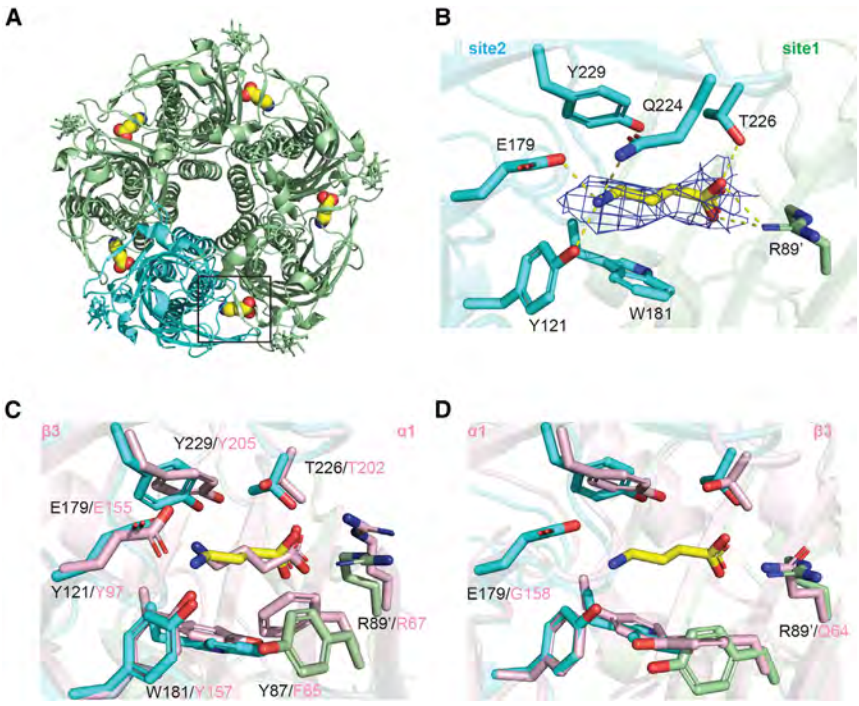

Figure 4. GABA-binding sites on GABRP$_\Delta$

(A) View of the receptor from the extracellular side, with GABA shown as spheres.

(B) GABA density in the GABA-bound GABRP$_\Delta$ complex cryo-EM reconstruction. GABA is bound to both protomers at site 1 (R89′, green) and site 2 (E179, cyan).

(C) Superposition of the GABA-binding site of GABRP$_\Delta$ with the GABA-binding pocket of GABA$_A$R α1β3γ2L (β3/α1 interface) (pink, PDB: 6HUJ).[32] The binding pocket of homomeric GABRP maintains the interactions found at the β3/α1 interface.

(D) Superposition of the GABA-binding site of GABRP$_\Delta$, with the non-binding subunit interface α1/β3 of the GABA receptor α1β3γ2L (pink, PDB: 6HUJ).[32]

the ECD center of mass (Figures S5A and S5B), minimizing the rotational inertia and thus reducing the energy required for the ligand to stabilize the active state conformation.

GABRP signal transduction

Unique to the π subunit of GABA$_A$Rs is its ability to stimulate cancer growth through MAPK/ERK signaling. Although our GABRP cryo-EM structures reveal a clear GABA-induced transition that can accommodate Cl^- passage, the link to ERK activation remains uncharacterized. Therefore, we tested whether channel opening is required for GABRP's signal transduction to ERK with the GABA$_A$R-pore-blocking picrotoxin (PTX-A). PTX-A treatment diminished GABA-stimulated ERK activity (Figure 6A), suggesting that GABRP signaling to ERK requires channel opening.

To further investigate GABRP's link to ERK activity, we used our GABRP$_\Delta$ stable cells—which show robust pERK in response to GABA—to examine global changes in the phosphoproteome in response to GABA. Collectively, a total of 36,589 phosphosites of 5,898 phosphoproteins were measured by a reproducible data-independent acquisition (DIA) mass spectrometry method.[34] Compared with non-stimulated cells, GABA-stimulated cells showed phosphoprotein enrichment in numerous signaling molecules, including ERK1/2 (pY204 and pY187), as expected (Figures S6A–S6F). Many of the significant changes occur in proteins related to membrane receptor signaling. In particular, pathway components often associated with G-protein signaling are prominent, including GPRIN1 (pS895), TRIO (pS2455 and pS2459), PLCβ3 (pS537), and multiple GEFs and GAPs (Figure 6B).

To ascertain whether heterotrimeric G-protein signaling is the underlying mechanism for ERK activation associated with GABRP, we examined the effects of two selective inhibitors: pertussis toxin (PTX-B), a Gαi/o-selective inhibitor, and FR900359, an inhibitor selective for Gαq/11. Treatment with PTX-B at a concentration of 1 μg/mL effectively inhibited GABA-induced ERK phosphorylation in GABRP$_\Delta$ stable cells (Figure 6C). In contrast, FR900359, even at a concentration of 10 μM, showed no such inhibitory effect (Figure S7A). These results indicate that, similar to metabotropic GABA$_B$ receptors, GABRP transduces signals via a Gαi/o pathway.

It was intriguing to find Gαi/o signaling important for GABRP's ERK activation, especially because GABA$_B$Rs use this pathway. Prior reports demonstrated that GABA$_A$Rs can help transport GABA$_B$R subunits to the cell surface and potentially form functional complexes.[35–37] Therefore, to investigate whether the Gαi/o signaling was originating from either GABRP or GABA$_B$Rs (chaperoned by GABRP), we tested the effect of GABAR-specific agonists. The GABA$_A$R-specific agonist muscimol (10 mM) was able to stimulate ERK in GABRP$_\Delta$ stable cells (Figure 6D), whereas the GABA$_B$R-specific agonist baclofen (10 mM) did not induce ERK signaling in the same cells (Figure 6D). These findings are consistent with GABA regulating Gαi/o signaling through GABRP and not through GABA$_B$Rs.

GABRP signals to ERK through Gβγ and PI3Kγ

Having established a critical role for Gαi/o in GABRP-induced ERK signaling, we sought to discern whether the signal originates directly from the alpha subunit (Gαi/o) or the beta and gamma subunits (Gβγ). To investigate this, we employed gallein, a selective Gβγ subunit inhibitor. Remarkably, gallein could completely block GABRP-dependent ERK phosphorylation (Figure 6E). These results suggest that Gαi/o activation and subsequent dissociation of the Gβγ subunits are key steps that lead to ERK signaling.

After identifying Gβγ as the essential subunits linking GABRP to ERK activity, we sought to further examine the pathway. Prior studies demonstrate that Gβγ can directly interact with PI3Kγ to

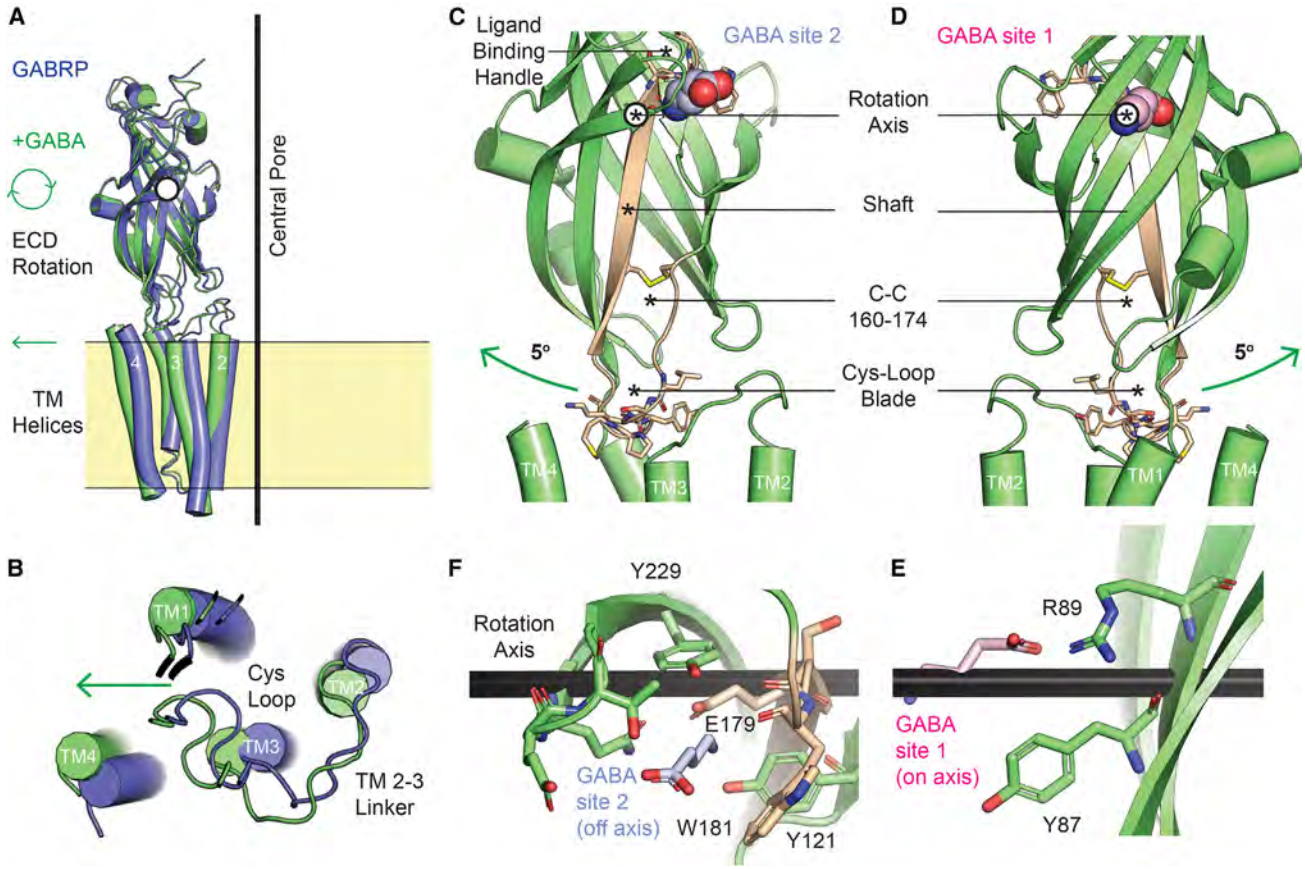

Figure 5. Structural basis of GABA-induced GABRP channel opening

(A) Overlay of a single $GABRP_{\Delta}$ protomer from unliganded (blue) and GABA-bound (green) structures reveals a clockwise ECD rotation about an axis parallel to the membrane (white circle). The ECD rotation is coupled to movement of the extracellular ends of the TM domains directed away from the central pore.

(B) A view of the extracellular side of the four TM helices shows an ~3 Å movement directed away from the center of the pore in the GABA-bound structure.

(C and D) Views of opposing GABRP protomers as in Figure 4, each showing opposite sides of the protomer. GABA site 1 shown in (D) and GABA site 2 in (C). The ECD axis of rotation is perpendicular to the page as in (A) (white circles). The β-strand shaft passes through the rotation axis, linking the GABA-binding handle to the Cys-loop blade. The hydrophobic blade sits in the middle of the four TM helices on the extracellular surface.

(E) Detailed view (90° rotation from D) of GABA binding at site 1. GABA bound at this site falls directly on the rotation axis (black rod).

(F) Detailed view (90° rotation from C) of GABA binding to the handle at site 2. GABA binding is offset to the rotation axis (black rod).

induce ERK signaling.[38–40] Therefore, we tested whether the PI3Kγ-selective inhibitor (AS-041164) could decouple GABRP stimulation from ERK activity. Indeed, we see that 1 μM AS-041164 completely abolishes the ERK phosphorylation induced by 10 μM GABA (Figure 6F). These results delineate a clear path from GABRP to ERK activity.

Extracellular inhibition of GABRP

The discovery that GABRP forms a functional homomeric channel, which actively signals to ERK, presents an intriguing possibility: selective inhibition of GABRP could effectively limit associated ERK activity. Employing phage display technology, we generated an antibody specifically targeting the ECD of GABRP (as detailed in STAR Methods). This antibody, designated C11-IgG, exhibited high-affinity binding to GABRP's ECD and successfully identified GABRP on the cell surface of GABRP-stable 293 cells (Figure S7B). Based on our finding that C11-IgG inhibits GABRP's ion channel function at supraphysiologic GABA concentrations (Figure 1B), we investigated whether it could also modulate GABA-induced ERK activity. Remarkably, at a concentration of 20 nM, C11-IgG completely abolished ERK activity stimulated by 10 μM GABA (Figure 6G). Recently, the mechanism of action of inhibitory autoantibodies targeting $GABA_AR$s have shown that they either block GABA binding or benzodiazepine binding.[41] Although the precise mechanism of action of C11-IgG warrants further exploration, our findings demonstrate that extracellular targeting of GABRP can effectively control its ability to signal to ERK.

Impact of GABRP signal inhibition in cancer cells

Having established that GABRP induces ERK signaling in an exogenously expressing stable cell system, we aimed to assess the impact of GABRP signal inhibition in cancer cells. Previously, we demonstrated that knockdown of GABRP impairs growth in breast cancer cell lines.[10] To further investigate this, we tested inhibition in two breast cancer cell lines: MDA-MB-468, which

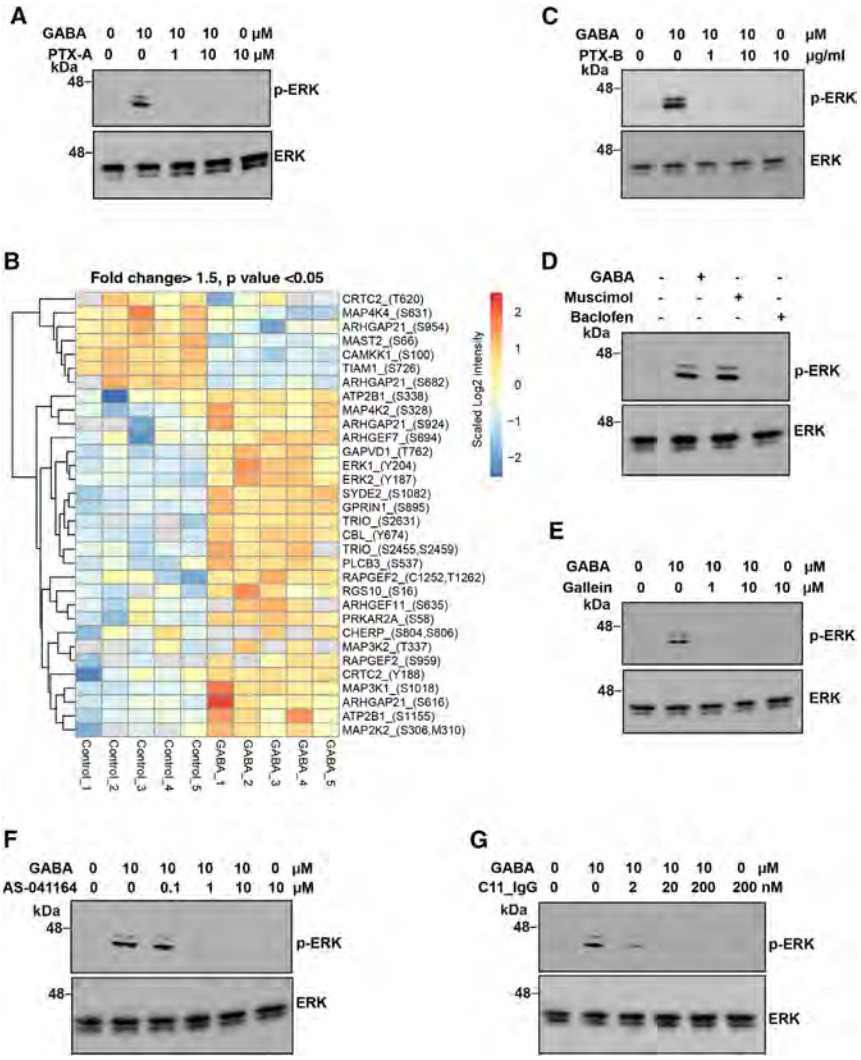

Figure 6. GABRP activation of ERK requires channel opening and G-protein signaling

(A) The $GABA_AR$-channel-blocking toxin, picrotoxin (PTX-A), inhibits GABA-induced GABRP signaling that leads to phosphorylation of ERK1/2.

(B) Heatmap of significant phosphorylation sites induced by GABA treatment of HEK293 cells stably expressing $GABRP_\Delta$, colored by intensity and compared with control. Multiple significant changes in G-protein-related molecules are prominent.

(C) The selective Gαi/o inhibitory toxin, pertussis toxin (PTX-B), prevents GABA-induced GABRP signaling that leads to phosphorylation of ERK1/2.

(D) The $GABA_AR$-selective agonist muscimol leads to ERK phosphorylation in HEK293 cells stably expressing $GABRP_\Delta$, whereas the $GABA_BR$-selective agonist baclofen does not induce ERK phosphorylation.

(E) The selective Gβγ inhibitory toxin, gallein, prevents the phosphorylation of ERK1/2 induced by GABA through GABRP.

(F) Selective inhibition of PI3Kγ prevents the phosphorylation of ERK1/2 induced by GABA through GABRP.

(G) A GABRP antibody (C11-IgG) prevents the phosphorylation of ERK1/2 induced by GABA.

exhibits high GABRP expression, and MDA-MB-231, which has lower levels of GABRP expression.[10] Consistent with their GABRP expression levels, C11-IgG significantly reduced the viability of MDA-MB-468 cells more than MDA-MB-231 cells (Figures 7A and 7B). Similarly, gallein and AS-041164 treatments reduced cancer cell viability, with a more pronounced effect observed in the high GABRP-expressing MDA-MB-468 cells (Figures 7C–7F). Together, these data demonstrate that inhibition of the GARP signaling axis in cancer cells can have a profound effect on cell viability.

DISCUSSION

Since its discovery more than a quarter century ago, GABRP has been thought to be incapable of forming homopentameric channels and incapable of binding to $GABA_AR$ agonists.[9] Recent focus has been on GABRP's importance in cancer and its ability to signal to ERK, thus regulating cancer cell growth[12,17]—bringing renewed interest into GABRP's mechanism of action. Our studies unexpectedly show that GABRP can function independently as an anion channel in a GABA-dependent manner. Our structural work demonstrates that GABRP can form homopentameric channels that maintain a conserved GABA-binding pocket. Additionally, visualizing GABRP channels in a native membrane environment allowed us to define the structural details that provide a clear view of how GABA regulates channel opening. These structures represent the resting-to-active transition for any $GABA_AR$. The vast majority of prior $GABA_AR$ structures captured desensitized states regardless of GABA binding—making a clear understanding of how GABA induces channel opening difficult. The rotation of GABRP's ECD from a resting-to-active state can be schematized as a rowing mechanism (Figure 7G). GABA binds at the "seat" position (site 1, R89) of one GABRP protomer and then engages the handle (site 2, E179) of an adjacent protomer. This causes the shaft and blade to rotate about the ECD axis (oar lock). The rotation of the blade draws the associated TM domains away from the center pore, opening the channel.

The GABA-induced GABRP channel opening we describe is also important for GABRP signal transduction. We show that the $GABA_AR$-pore-blocking toxin PTX-A can diminish GABRP's ability to signal to ERK. Through phosphoproteomic analysis of GABRP activation, we revealed an unexpected link to G-protein signaling. We show that Gαi/o inhibition by PTX-B can diminish GABRP-stimulated ERK activation. Thus, blocking the channel pore (PTX-A) or inhibiting Gαi/o (PTX-B) prevents GABRP-induced ERK activation (Figure 7G). Although not

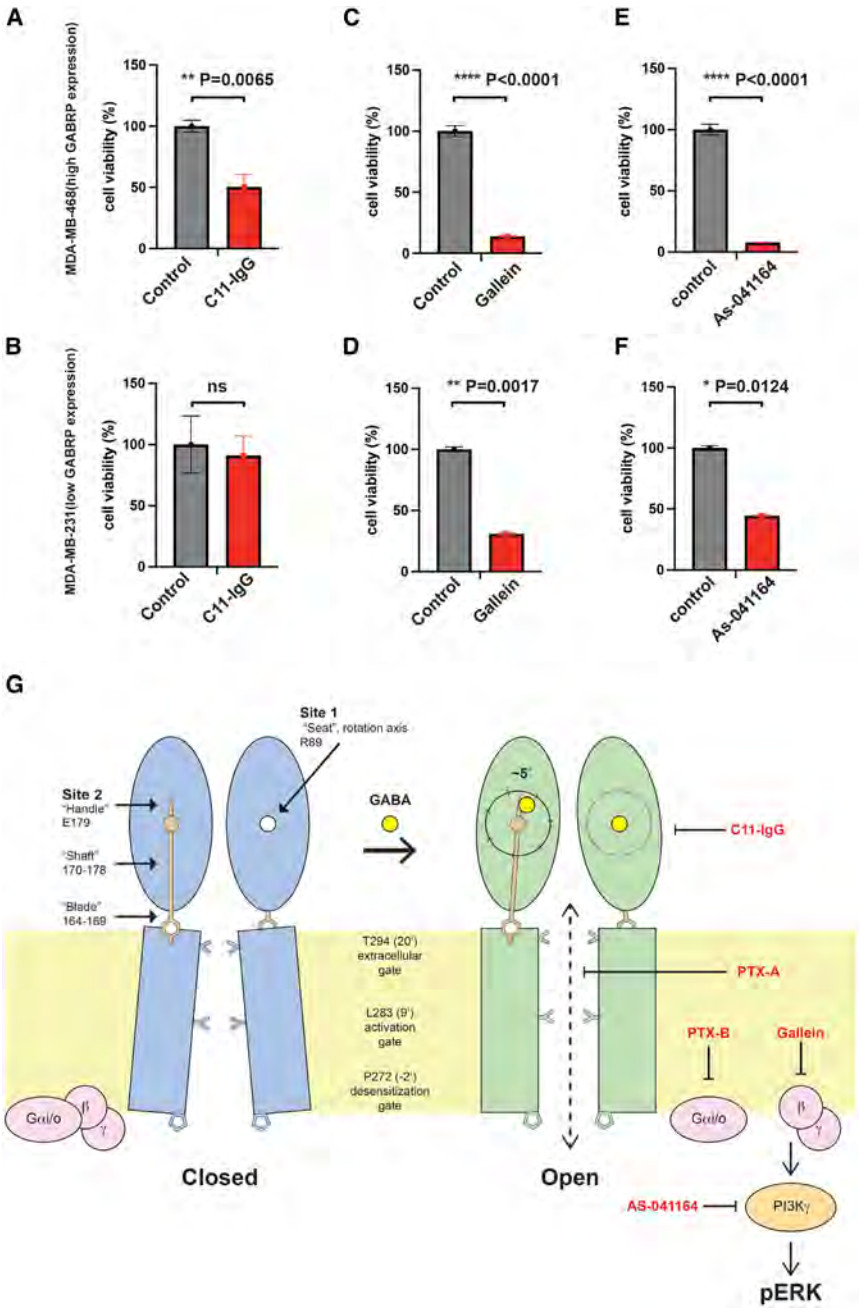

Figure 7. GABRP-signaling axis inhibition on breast cancer cells

(A and B) C11-IgG treatment of MDA-MB-468 and MDA-MB-231 cell lines, $n = 3$, error bars indicated mean ± SEM. Significant p values reported from t test.

(C and D) Gallein (Gβγ inhibitor) treatment of MDA-MB-468 and MDA-MB-231 cell lines, $n = 3$, error bars indicated mean ± SEM. Significant p values reported from t test.

(E and F) As-041164 (PI3Kγ inhibitor) treatment of MDA-MB-468 and MDA-MB-231 cell lines, $n = 3$, error bars indicated mean ± SEM. Significant p values reported from t test. NS, not statistically significant.

(G) Schema for GABA-induced transitions of GABRP. For simplicity, only opposing protomers are shown. In the unliganded resting state (blue), GABRP's channel is closed at multiple gates, including T294 and L283. GABA binds to site 1, the seat, which represents a special position that passes through the ECD rotation axis (denoted as a white circle). The same GABA molecule simultaneously engages site 2 at the handle of another molecule in the pentamer, and this site is offset from the rotation axis of that protomer. This mode of binding stabilizes the rotated state of the ECD. The resulting ECD rotation is translated to the extracellular ends of the TMs though the Cys-loop blade via the shaft, causing the TMs to be drawn directly away from the central pore in a concerted way. Channel opening is coupled to activation of Gαi/o signaling that leads to ERK phosphorylation. However, chloride flux only occurs at supraphysiologic GABA concentrations. Different inhibitors (red) at multiple steps can prevent phosphorylation of ERK induced by GABA.

common, metabotropic activity of ion channels has been described previously. For example, the nicotinic acetylcholine receptors (nAChRs) have been shown to couple directly to multiple G proteins to control axon growth.[42] Additionally, ionotropic glutamate receptors (AMPARs) have been shown to activate ERK in a PTX-B-sensitive manner[43] and to directly interact with Gα proteins.[44]

Our discovery that an antibody targeting GABRP can inhibit its ability to signal to ERK has significant implications for cancer research. Given the well-documented involvement of the GABRP-ERK signaling axis in cancer progression, our findings suggest potential therapeutic strategies. Our pathway analysis reveals that Gβγ- or PI3Kγ-specific inhibition can block GABRP-linked ERK activity. Remarkably, a PI3Kγ-selective inhibitor (eganelisib, IPI-549) has recently received fast-track designation by the FDA for use in triple-negative breast cancers (TNBCs)-MARIO-3 study (Clinical trial: NCT03961698)—cancers with overexpression of GABRP. It is thought that eganelisib solely impacts an immune-related pathway and does not function directly on cancer cells.[45] However, in light of our results, and the high expression of PI3Kγ in a subset of TNBCs,[46] we believe that a potentially overlooked mechanism of action for eganelisib could be by directly blocking a GABRP-directed growth pathway on GABRP-expressing cancer cells.

Our findings reveal that, despite its channel-like structure, GABRP primarily signals to ERK via G-protein activation, more similar to type-B GABA receptors, rather than functioning as an ion channel. This decoupling helps reconcile how activation of an inhibitory anion channel drives growth in numerous cancers. Further investigation is needed to determine how GABRP specifically directs G-protein activity. Together, our model of GABRP channel regulation by GABA and its signaling points to

new opportunities to inhibit its activity in GABRP-associated cancers.

Limitations of the study

Although this study addresses several longstanding mysteries regarding the unique nature of GABRP, there are important aspects that remain unexplored. Specifically, our study does not elucidate the precise mechanisms by which GABA-induced structural transitions initiate G-protein signaling. Understanding this mechanistic link is crucial for fully characterizing GABRP's role in cellular signaling pathways.

RESOURCE AVAILABILITY

Lead contact

Further information and requests for resource and reagents should be directed to and will be fulfilled by the lead contact, Daryl E. Klein (daryl.klein@yale.edu).

Materials availability

All unique/stable reagents generated in this study are available from the lead contact upon request.

Data and code availability

- The mass spectrometry raw dataset has been deposited to the ProteomeXchange Consortium via the PRIDE partner repository with the dataset identifier PXD044482.
- The atomic coordinates for GABRP, with and without GABA, have been deposited in the PDB with accession codes PDB: 8VV0 and 8VSZ, respectively. The EM maps of GABRP, with and without GABA, have been deposited in the EMDB with accession codes EMD-43546 and EMD-43512, respectively.
- The paper does not report original code.
- All materials are available from the corresponding authors upon request.

ACKNOWLEDGMENTS

We thank the staff in the Laboratory for BioMolecular Structure (LBMS). The Laboratory for BioMolecular Structure (LBMS) is supported by the DOE Office of Biological and Environmental Research (KP1607011). This work was supported by the NIH (grants RM1GM149406 [D.E.K. and Y.L.] and NS102239 [L.K.K.]) and the Breast Cancer Investigator award BCRF-22-133 (L.P.).

AUTHOR CONTRIBUTIONS

Y.W. conducted all structural and signaling assays under the guidance of D.E.K. and L.P. Y.Z. carried out the electrophysiological experiments under the guidance of L.K.K. J.Z. aided in the cryo-EM data collection and workflow. W.L. and B.S. performed the mass spectrometry and phosphoproteomics experiment and its initial data analysis under the supervision of Y.L. T.L. and H.L. supported the protein production and assays. Y.W. and D.E.K. analyzed data and prepared the manuscript with input from all authors.

DECLARATION OF INTERESTS

The authors declare no competing interests.

STAR★METHODS

Detailed methods are provided in the online version of this paper and include the following:

SUPPLEMENTAL INFORMATION

Supplemental information can be found online at https://doi.org/10.1016/j.molcel.2024.11.016.

Received: February 8, 2024
Revised: May 3, 2024
Accepted: November 11, 2024
Published: December 5, 2024

REFERENCES

1. Fritschy, J.M., and Mohler, H. (1995). Gaba(a)-Receptor Heterogeneity in the Adult-Rat Brain - Differential Regional and Cellular-Distribution of 7 Major Subunits. J. Comp. Neurol. *359*, 154–194. https://doi.org/10.1002/cne.903590111.
2. Olsen, R.W., and Sieghart, W. (2009). GABA(A) receptors: Subtypes provide diversity of function and pharmacology. Neuropharmacology *56*, 141–148. https://doi.org/10.1016/j.neuropharm.2008.07.045.
3. Chua, H.C., and Chebib, M. (2017). GABAA Receptors and the Diversity in their Structure and Pharmacology. In Advances in Pharmacology, D.P. Geraghty and L.D. Rash, eds. (Academic Press), pp. 1–34. https://doi.org/10.1016/bs.apha.2017.03.003.
4. Sigel, E., and Steinmann, M.E. (2012). Structure, function, and modulation of GABA(A) receptors. J. Biol. Chem. *287*, 40224–40231. https://doi.org/10.1074/jbc.R112.386664.
5. Farrar, S.J., Whiting, P.J., Bonnert, T.P., and McKernan, R.M. (1999). Stoichiometry of a ligand-gated ion channel determined by fluorescence energy transfer. J. Biol. Chem. *274*, 10100–10104. https://doi.org/10.1074/jbc.274.15.10100.
6. Chang, Y., Wang, R., Barot, S., and Weiss, D.S. (1996). Stoichiometry of a recombinant GABAA receptor. J. Neurosci. *16*, 5415–5424. https://doi.org/10.1523/JNEUROSCI.16-17-05415.1996.
7. Tretter, V., Ehya, N., Fuchs, K., and Sieghart, W. (1997). Stoichiometry and assembly of a recombinant GABAA receptor subtype. J. Neurosci. *17*, 2728–2737. https://doi.org/10.1523/JNEUROSCI.17-08-02728.1997.
8. Terunuma, M. (2018). Diversity of structure and function of GABA(B) receptors: a complexity of GABA(B)-mediated signaling. Proc. Jpn. Acad. Ser. B Phys. Biol. Sci. *94*, 390–411. https://doi.org/10.2183/pjab.94.026.
9. Hedblom, E., and Kirkness, E.F. (1997). A novel class of GABAA receptor subunit in tissues of the reproductive system. J. Biol. Chem. *272*, 15346–15350. https://doi.org/10.1074/jbc.272.24.15346.
10. Wali, V.B., Patwardhan, G.A., Pelekanou, V., Karn, T., Cao, J., Ocana, A., Yan, Q., Nelson, B., Hatzis, C., and Pusztai, L. (2019). Identification and Validation of a Novel Biologics Target in Triple Negative Breast Cancer. Sci. Rep. *9*, 14934. https://doi.org/10.1038/s41598-019-51453-w.
11. Li, X.Y., Wang, H.R., Yang, X., Wang, X.Q., Zhao, L.A., Zou, L., Yang, Q., Hou, Z.L., Tan, J., Zhang, H.L., et al. (2021). GABRP sustains the stemness of triple-negative breast cancer cells through EGFR signaling. Cancer Lett. *514*, 90–102. https://doi.org/10.1016/j.canlet.2021.04.028.

12. Sizemore, G.M., Sizemore, S.T., Seachrist, D.D., and Keri, R.A. (2014). GABA(A) receptor pi (GABRP) stimulates basal-like breast cancer cell migration through activation of extracellular-regulated kinase 1/2 (ERK1/2). J. Biol. Chem. *289*, 24102–24113. https://doi.org/10.1074/jbc.M114.593582.

13. Takehara, A., Hosokawa, M., Eguchi, H., Ohigashi, H., Ishikawa, O., Nakamura, Y., and Nakagawa, H. (2007). Gamma-aminobutyric acid (GABA) stimulates pancreatic cancer growth through overexpressing GABAA receptor pi subunit. Cancer Res. *67*, 9704–9712. https://doi.org/10.1158/0008-5472.CAN-07-2099.

14. Jiang, S.H., Zhu, L.L., Zhang, M., Li, R.K., Yang, Q., Yan, J.Y., Zhang, C., Yang, J.Y., Dong, F.Y., Dai, M., et al. (2019). GABRP regulates chemokine signalling, macrophage recruitment and tumour progression in pancreatic cancer through tuning KCNN4-mediated Ca2+ signalling in a GABA-independent manner. Gut *68*, 1994–2006. https://doi.org/10.1136/gutjnl-2018-317479.

15. Meng, Y., Li, R., Geng, S., Chen, W., Jiang, W., Li, Z., Hao, J., and Xu, Z. (2024). GABRP Promotes the Metastasis of Pancreatic Cancer by Activation of the MEK/ERK Signaling Pathway. Biochem. Genet. *62*, 242–253. https://doi.org/10.1007/s10528-023-10410-z.

16. Sung, H.Y., Yang, S.D., Ju, W., and Ahn, J.H. (2017). Aberrant epigenetic regulation of GABRP associates with aggressive phenotype of ovarian cancer. Exp. Mol. Med. *49*, e335. https://doi.org/10.1038/emm.2017.62.

17. Juvale, I.I.A., Hassan, Z., and Has, A.T.C. (2021). The Emerging Roles of π Subunit-Containing GABA(A) Receptors in Different Cancers. Int. J. Med. Sci. *18*, 3851–3860. https://doi.org/10.7150/ijms.60928.

18. Yang, Y., Ren, L., Li, W., Zhang, Y., Zhang, S., Ge, B., Yang, H., Du, G., Tang, B., Wang, H., et al. (2023). GABAergic signaling as a potential therapeutic target in cancers. Biomed. Pharmacother. *161*, 114410. https://doi.org/10.1016/j.biopha.2023.114410.

19. Neelands, T.R., and Macdonald, R.L. (1999). Incorporation of the pi subunit into functional gamma-aminobutyric acid(A) receptors. Mol. Pharmacol. *56*, 598–610. https://doi.org/10.1124/mol.56.3.598.

20. Pritchett, D.B., Sontheimer, H., Gorman, C.M., Kettenmann, H., Seeburg, P.H., and Schofield, P.R. (1988). Transient expression shows ligand gating and allosteric potentiation of GABAA receptor subunits. Science *242*, 1306–1308. https://doi.org/10.1126/science.2848320.

21. Kasaragod, V.B., Mortensen, M., Hardwick, S.W., Wahid, A.A., Dorovykh, V., Chirgadze, D.Y., Smart, T.G., and Miller, P.S. (2022). Mechanisms of inhibition and activation of extrasynaptic αβ GABA(A) receptors. Nature *602*, 529–533. https://doi.org/10.1038/s41586-022-04402-z.

22. Phulera, S., Zhu, H.T., Yu, J., Claxton, D.P., Yoder, N., Yoshioka, C., and Gouaux, E. (2018). Cryo-EM structure of the benzodiazepine-sensitive α1β1γ2S tri-heteromeric GABAA receptor in complex with GABA. eLife *7*, e39383. https://doi.org/10.7554/eLife.39383.

23. Miller, P.S., and Aricescu, A.R. (2014). Crystal structure of a human GABAA receptor. Nature *512*, 270–275. https://doi.org/10.1038/nature13293.

24. Zhu, S., Noviello, C.M., Teng, J., Walsh, R.M., Jr., Kim, J.J., and Hibbs, R.E. (2018). Structure of a human synaptic GABA(A) receptor. Nature *559*, 67–72. https://doi.org/10.1038/s41586-018-0255-3.

25. Akk, G., Shin, D.J., Germann, A.L., and Steinbach, J.H. (2018). GABA Type A Receptor Activation in the Allosteric Coagonist Model Framework: Relationship between EC(50) and Basal Activity. Mol. Pharmacol. *93*, 90–100. https://doi.org/10.1124/mol.117.110569.

26. Gielen, M., Barilone, N., and Corringer, P.J. (2020). The desensitization pathway of GABA(A) receptors, one subunit at a time. Nat. Commun. *11*, 5369. https://doi.org/10.1038/s41467-020-19218-6.

27. Dimitrova, V., Song, S., Karagiaridi, A., Marand, A., and Pinkett, H. (2023). Detergent Alternatives: Membrane Protein Purification Using Synthetic Nanodisc Polymers. Protein Sci. *32*, e21856.

28. Pravda, L., Sehnal, D., Toušek, D., Navrátilová, V., Bazgier, V., Berka, K., Svobodová Vareková, R., Koca, J., and Otyepka, M. (2018). MOLEonline: a web-based tool for analyzing channels, tunnels and pores (2018 update). Nucleic Acids Res. *46*, W368–W373. https://doi.org/10.1093/nar/gky309.

29. Smart, O.S., Neduvelil, J.G., Wang, X., Wallace, B.A., and Sansom, M.S. (1996). HOLE: a program for the analysis of the pore dimensions of ion channel structural models. J. Mol. Graph. *14*, 354–360. 376. https://doi.org/10.1016/s0263-7855(97)00009-x.

30. Laverty, D., Desai, R., Uchański, T., Masiulis, S., Stec, W.J., Malinauskas, T., Zivanov, J., Pardon, E., Steyaert, J., Miller, K.W., et al. (2019). Cryo-EM structure of the human α1β3γ2 GABAA receptor in a lipid bilayer. Nature *565*, 516–520. https://doi.org/10.1038/s41586-018-0833-4.

31. Sente, A., Desai, R., Naydenova, K., Malinauskas, T., Jounaidi, Y., Miehling, J., Zhou, X., Masiulis, S., Hardwick, S.W., Chirgadze, D.Y., et al. (2022). Differential assembly diversifies GABA(A) receptor structures and signalling. Nature *604*, 190–194. https://doi.org/10.1038/s41586-022-04517-3.

32. Masiulis, S., Desai, R., Uchański, T., Serna Martin, I., Laverty, D., Karia, D., Malinauskas, T., Zivanov, J., Pardon, E., Kotecha, A., et al. (2019). GABA(A) receptor signalling mechanisms revealed by structural pharmacology. Nature *565*, 454–459. https://doi.org/10.1038/s41586-018-0832-5.

33. Kim, J.J., and Hibbs, R.E. (2021). Direct Structural Insights into GABA(A) Receptor Pharmacology. Trends Biochem. Sci. *46*, 502–517. https://doi.org/10.1016/j.tibs.2021.01.011.

34. Zhou, W.P., Li, W.X., Wang, S.S., Salovska, B., Hu, Z.Y., Tao, B., Di, Y., Punyamurtula, U., Turk, B.E., Sessa, W.C., et al. (2023). An optogenetic-phosphoproteomic study reveals dynamic Akt1 signaling profiles in endothelial cells. Nat. Commun. *14*, 3803. https://doi.org/10.1038/s41467-023-39514-1.

35. Balasubramanian, S., Teissére, J.A., Raju, D.V., and Hall, R.A. (2004). Hetero-oligomerization between GABAA and GABAB receptors regulates GABAB receptor trafficking. J. Biol. Chem. *279*, 18840–18850. https://doi.org/10.1074/jbc.M313470200.

36. Jung, C., Fernández-Dueñas, V., Plata, C., Garcia-Elias, A., Ciruela, F., Fernández-Fernández, J.M., and Valverde, M.A. (2018). Functional coupling of GABAA/B receptors and the channel TRPV4 mediates rapid progesterone signaling in the oviduct. Sci. Signal. *11*, eaam6558. https://doi.org/10.1126/scisignal.aam6558.

37. Negri, S., Scolari, F., Vismara, M., Brunetti, V., Faris, P., Terribile, G., Sancini, G., Berra-Romani, R., and Moccia, F. (2022). GABA(A) and GABA(B) Receptors Mediate GABA-Induced Intracellular Ca(2+) Signals in Human Brain Microvascular Endothelial Cells. Cells *11*, 3860. https://doi.org/10.3390/cells11233860.

38. Vadas, O., Dbouk, H.A., Shymanets, A., Perisic, O., Burke, J.E., Abi Saab, W.F., Khalil, B.D., Harteneck, C., Bresnick, A.R., Nürnberg, B., et al. (2013). Molecular determinants of PI3Kgamma-mediated activation downstream of G-protein-coupled receptors (GPCRs). Proc. Natl. Acad. Sci. USA *110*, 18862–18867. https://doi.org/10.1073/pnas.1304801110.

39. Brock, C., Schaefer, M., Reusch, H.P., Czupalla, C., Michalke, M., Spicher, K., Schultz, G., and Nürnberg, B. (2003). Roles of G beta gamma in membrane recruitment and activation of p110 gamma/p101 phosphoinositide 3-kinase gamma. J. Cell Biol. *160*, 89–99. https://doi.org/10.1083/jcb.200210115.

40. Lopez-Ilasaca, M., Crespo, P., Pellici, P.G., Gutkind, J.S., and Wetzker, R. (1997). Linkage of G protein-coupled receptors to the MAPK signaling pathway through PI 3-kinase gamma. Science *275*, 394–397. https://doi.org/10.1126/science.275.5298.394.

41. Noviello, C.M., Kreye, J., Teng, J., Prüss, H., and Hibbs, R.E. (2022). Structural mechanisms of GABA(A) receptor autoimmune encephalitis. Cell *185*, 2469–2477.e2413. https://doi.org/10.1016/j.cell.2022.06.025.

42. Kabbani, N., Nordman, J.C., Corgiat, B.A., Veltri, D.P., Shehu, A., Seymour, V.A., and Adams, D.J. (2013). Are nicotinic acetylcholine receptors coupled to G proteins? BioEssays *35*, 1025–1034. https://doi.org/10.1002/bies.201300082.

43. Wang, Y., and Durkin, J.P. (1995). alpha-amino-3-hydroxy-5-methyl-4-isoxazolepropionic acid, but not N-methyl-D-aspartate, activates mitogen-activated protein kinase through G-protein beta gamma subunits in rat cortical neurons. J. Biol. Chem. *270*, 22783–22787. https://doi.org/10.1074/jbc.270.39.22783.

44. Wang, Y., Small, D.L., Stanimirovic, D.B., Morley, P., and Durkin, J.P. (1997). AMPA receptor-mediated regulation of a Gi-protein in cortical neurons. Nature *389*, 502–504. https://doi.org/10.1038/39062.

45. Kaneda, M.M., Messer, K.S., Ralainirina, N., Li, H., Leem, C.J., Gorjestani, S., Woo, G., Nguyen, A.V., Figueiredo, C.C., Foubert, P., et al. (2016). PI3Kgamma is a molecular switch that controls immune suppression. Nature *539*, 437–442. https://doi.org/10.1038/nature19834.

46. Chang, J., Hong, L., Liu, Y., Pan, Y., Yang, H., Ye, W., Xu, K., Li, Z., and Zhang, S. (2020). Targeting PIK3CG in Combination with Paclitaxel as a Potential Therapeutic Regimen in Claudin-Low Breast Cancer. Cancer Manag. Res. *12*, 2641–2651. https://doi.org/10.2147/CMAR.S250171.

47. Punjani, A., Rubinstein, J.L., Fleet, D.J., and Brubaker, M.A. (2017). cryoSPARC: algorithms for rapid unsupervised cryo-EM structure determination. Nat. Methods *14*, 290–296. https://doi.org/10.1038/nmeth.4169.

48. Emsley, P., Lohkamp, B., Scott, W.G., and Cowtan, K. (2010). Features and development of Coot. Acta Crystallogr. D Biol. Crystallogr. *66*, 486–501. https://doi.org/10.1107/S0907444910007493.

49. Afonine, P.V., Poon, B.K., Read, R.J., Sobolev, O.V., Terwilliger, T.C., Urzhumtsev, A., and Adams, P.D. (2018). Real-space refinement in PHENIX for cryo-EM and crystallography. Acta Crystallogr. D Struct. Biol. *74*, 531–544. https://doi.org/10.1107/S2059798318006551.

50. Pettersen, E.F., Goddard, T.D., Huang, C.C., Couch, G.S., Greenblatt, D.M., Meng, E.C., and Ferrin, T.E. (2004). UCSF chimera - A visualization system for exploratory research and analysis. J. Comput. Chem. *25*, 1605–1612. https://doi.org/10.1002/jcc.20084.

51. Miller, P.S., Scott, S., Masiulis, S., De Colibus, L., Pardon, E., Steyaert, J., and Aricescu, A.R. (2017). Structural basis for GABA(A) receptor potentiation by neurosteroids. Nat. Struct. Mol. Biol. *24*, 986–992. https://doi.org/10.1038/nsmb.3484.

52. Morales-Perez, C.L., Noviello, C.M., and Hibbs, R.E. (2016). Manipulation of Subunit Stoichiometry in Heteromeric Membrane Proteins. Structure *24*, 797–805. https://doi.org/10.1016/j.str.2016.03.004.

53. Aricescu, A.R., and Owens, R.J. (2013). Expression of recombinant glycoproteins in mammalian cells: towards an integrative approach to structural biology. Curr. Opin. Struct. Biol. *23*, 345–356. https://doi.org/10.1016/j.sbi.2013.04.003.

54. Reeves, P.J., Callewaert, N., Contreras, R., and Khorana, H.G. (2002). Structure and function in rhodopsin: high-level expression of rhodopsin with restricted and homogeneous N-glycosylation by a tetracycline-inducible N-acetylglucosaminyltransferase I-negative HEK293S stable mammalian cell line. Proc. Natl. Acad. Sci. USA *99*, 13419–13424. https://doi.org/10.1073/pnas.212519299.

55. Morin, A., Eisenbraun, B., Key, J., Sanschagrin, P.C., Timony, M.A., Ottaviano, M., and Sliz, P. (2013). Collaboration gets the most out of software. eLife *2*, e01456. https://doi.org/10.7554/eLife.01456.

56. Jumper, J., Evans, R., Pritzel, A., Green, T., Figurnov, M., Ronneberger, O., Tunyasuvunakool, K., Bates, R., Žídek, A., Potapenko, A., et al. (2021). Highly accurate protein structure prediction with AlphaFold. Nature *596*, 583–589. https://doi.org/10.1038/s41586-021-03819-2.

57. Varadi, M., Anyango, S., Deshpande, M., Nair, S., Natassia, C., Yordanova, G., Yuan, D., Stroe, O., Wood, G., Laydon, A., et al. (2022). AlphaFold Protein Structure Database: massively expanding the structural coverage of protein-sequence space with high-accuracy models. Nucleic Acids Res. *50*, D439–D444. https://doi.org/10.1093/nar/gkab1061.

58. Persson, H., Ye, W., Wernimont, A., Adams, J.J., Koide, A., Koide, S., Lam, R., and Sidhu, S.S. (2013). CDR-H3 diversity is not required for antigen recognition by synthetic antibodies. J. Mol. Biol. *425*, 803–811. https://doi.org/10.1016/j.jmb.2012.11.037.

59. Nelson, B., and Sidhu, S.S. (2012). Synthetic antibody libraries. Methods Mol. Biol. *899*, 27–41. https://doi.org/10.1007/978-1-61779-921-1_2.

60. Liu, Y.S., Mi, Y., Mueller, T., Kreibich, S., Williams, E.G., Van Drogen, A., Borel, C., Frank, M., Germain, P.L., Bludau, I., et al. (2019). Multi-omic measurements of heterogeneity in HeLa cells across laboratories. Nat. Biotechnol. *37*, 314–322. https://doi.org/10.1038/s41587-019-0037-y.

61. Gao, E., Li, W., Wu, C., Shao, W., Di, Y., and Liu, Y. (2021). Data-independent acquisition-based proteome and phosphoproteome profiling across six melanoma cell lines reveals determinants of proteotypes. Mol. Omics *17*, 413–425. https://doi.org/10.1039/d0mo00188k.

62. Bruderer, R., Bernhardt, O.M., Gandhi, T., Xuan, Y., Sondermann, J., Schmidt, M., Gomez-Varela, D., and Reiter, L. (2017). Optimization of Experimental Parameters in Data-Independent Mass Spectrometry Significantly Increases Depth and Reproducibility of Results. Mol. Cell. Proteomics *16*, 2296–2309. https://doi.org/10.1074/mcp.RA117.000314.

63. Perez-Riverol, Y., Csordas, A., Bai, J., Bernal-Llinares, M., Hewapathirana, S., Kundu, D.J., Inuganti, A., Griss, J., Mayer, G., Eisenacher, M., et al. (2019). The PRIDE database and related tools and resources in 2019: improving support for quantification data. Nucleic Acids Res. *47*, D442–D450. https://doi.org/10.1093/nar/gky1106.

STAR★METHODS

KEY RESOURCES TABLE

REAGENT or RESOURCE	SOURCE	IDENTIFIER
Antibodies		
Phospho-p44/42 MAPK (Erk1/2) (Thr202/Tyr204) (D13.14.4E)	Cell signaling Technology	Cat#:4370; RRID: AB_2315112
p44/42 MAPK (Erk1/2)	Cell signaling Technology	Cat#: 9102; RRID: AB_330744
Anti-rabbit IgG, HRP-linked Antibody	Cell signaling Technology	Cat#: 7074; RRID: AB_2099233
Strep-Tactin® HRP	IBA GmbH	Cat#: 2-1502-001
C11-IgG	This Study	N/A
Bacterial and virus strains		
DH5a competent cells	Lab stock	N/A
DH10Bac competent cells	Lab stock	N/A
Chemicals, peptides, and recombinant proteins		
SF900 II medium	Life Technologies	Cat#: 10902104
DMEM	Gibco	Cat#: 11995-065
RPIM1640	Gibco	Cat#: 11875085
Fetal Bovine Serum, qualified, heat inactivated	Gibco	Cat#: 16140-071
Trypsin-EDTA (0.05%), phenol red	Gibco	Cat#: 25300-054
Penicillin-Streptomycin	Sigma-Aldrich	Cat#: P4333
Lipofectamine 2000	Invitrogen	Cat#: 11668-019
Dimethyl sulfoxide (DMSO)	Sigma-Aldrich	Cat#: D2438
Protease/Phosphatase Inhibitor Cocktail (100X)	Cell Signaling Technology	Cat#: 5872
DPBS	Gibco	Cat#: 14190-250
cOmplete, EDTA-free PIC	Roche-Merck	Cat#:11873580001
FreeStyle™ 293 Expression Medium	Gibco	Cat#: 12338018
Opti-MEM I Reduced Serum Medium	Gibco	Cat#: 31985-088
γ-Aminobuturic Acid	Sigma	Cat#: A2129-100G
Puromycin	InvivoGen	Cat#: ant-pr-1
Valproic acid sodium salt	Thomas Scientific Holdings LLC DBA	Cat#: C977N40
4xLaemmli sample buffer	Biorad	Cat#: 1610747
Novex™ Tris-Glycine Mini Protein Gels, 4–20%	ThermoFisher Scientific	Cat#: XP04205BOX
ECL PRIME WESTERN BLOTTING DET	Amersham	Cat#: 17017131
SMALP200	Cube Biotech	Cat#: 182111
AS-041164	Cayman Chemical Company	Cat#: 13622-10
(+)-Baclofen (hydrochloride)	Cayman Chemical Company	Cat#:31595-10
Gallein	Cayman Chemical Company	Cat#: 16344-50
Muscimol	Cayman Chemical Company	Cat#: 13667-5
FR900359	Cayman Chemical Company	Cat#: 33666-250
Pertussis Toxin	R&D Systems INC	Cat#: 3097/50U
Picrotoxin powder	Thomas Scientific Holdings LLC DBA	Cat#: C964M60
Mini Trans-Blot® Filter Paper	Bio-Rad	Cat#: 1703932
Protein A Agarose Resin	GoldBio	Cat#: P-400-50
Immobilon-P Membrane, PVDF	EMD Millipore	Cat#: IPVH00010
Poly-D-Lysine	Life Technologies Corporation DBA Thermo Fisher Scientific	Cat#: A3890401
Critical commercial assays		
Strep-TactinXT 4 Flow	IBA Lifesciences GMBH	Cat#: 2-5030-010

(*Continued on next page*)

Continued		
REAGENT or RESOURCE	SOURCE	IDENTIFIER
CellTiter-Glo 2.0 Assay	Promega Corporation	Cat#: G9242
Superdex 200 Increase 10/300 GL	GE Healthcare Life Sciences	Cat#: 28990944
NEBuilder HiFi DNA Assembly Cloning Kit	New England Biolabs	Cat#: E5520S
Deposited data		
Cryo-EM map of Apo $GABRP_{\Delta}$	This Study	EMDB: EMD-43512
Cryo-EM map of GABA-bound $GABRP_{\Delta}$	This Study	EMDB: EMD-43546
Coordinates of Apo $GABRP_{\Delta}$	This Study	PDB: 8VSZ
Coordinates of GABA-bound $GABRP_{\Delta}$	This Study	PDB:8VV0
Experimental models: Cell lines		
HEK293	ATCC	Cat#: CRL-1573
MDA-MB-468	ATCC	Cat#: HTB-132
Expi293F GnTI- cells	Gibco	Cat#: A39240
Sf9	ATCC	Cat#: CRL-1711
HEK293 GABAA Receptor $\alpha1\beta2\gamma2$(long form) Cell Line	Sigma-Aldrich	Cat#: SCC461
Oligonucleotides		
GF-F	This Study	Sequence:ctcactataggctagcctcgaggccacc ATGAACTACAGCCTCCACTTGG
GF-R	This Study	Sequence:GACTCCAAGCACTACCTCTAG ACCCCCCGAATTCAAAATACATGTAG
Gdel-F	This Study	Sequence:TCTCAACCTGCACGCGCAGCA AATGTTGATCACTATTCCAAACTACTGTTTCC
Gdel-R	This Study	Sequence:TGCTGCGCGTGCAGGTTGAGA TAAGGAACTGTAGTGAGCAACTGC
Recombinant DNA		
$GABRP_{\Delta}$-pEZT-BM	This Study	N/A
$GABRP_{\Delta}$ -pLenti-Puro	This Study	N/A
GABRP-pLenti-Puro	This Study	N/A
Software and algorithms		
GraphPad Prism 9.4	GraphPad Software Inc	http://www.graphpad.com/scientific-software/prism/
EPU automated collection software	Thermo Fisher Scientific	https://www.thermofisher.com/us/en/home/electron-microscopy/products/software-em-3d-vis/epu-software.html#epu-3-software
CryoSPARC 4.0	Grant et al.[47]	https://cryosparc.com/
Coot	Emsley et al.[48]	https://www2.mrc-lmb.cam.ac.uk/personal/pemsley/coot/
PHENIX	Adams et al.[49]	https://phenix-online.org
HOLE	Smart et al.[29]	http://www.holeprogram.org
USCF Chimerax	Pettersen et al.[50]	https://www.cgl.ucsf.edu/chimerax/
Other		
ÄKTA pure 25 M	GE Healthcare	Cat#: 29018226
ChemiDoc MP Imaging System	Bio-Rad	Cat#: 17001402
HulaMixer™ Sample Mixer	Thermo Fisher	Cat#: 15920D
Quantifoil R11.2/1.3 Au 300 mesh	Electron microscopy Science	Cat#: Q3100AR1.3

EXPERIMENTAL MODEL AND STUDY PARTICIPANT DETAILS

The HEK293 GnTI^{-} suspension cells (Twin-strep-tagged $GABRP_{\Delta}$) were maintained in Gibco Freestyle ^{TM}293 expression medium (Thermo Fisher Scientific, Catalog #:12338026) with 1% fetal bovine serum and 1% non-essential amino acids (Gibco,

Catalog #: 11140076) in shaking incubators at 37 ℃, humid atmosphere and 8% CO2. HEK293(Twin-strep-tagged $GABRP_{\Delta}$ and GABRP) and HEK293 expressing $GABA_AR$ $\alpha1\beta2\gamma2$ (long form) were maintained in DMEM medium supplemented with 10% fetal bovine serum(FBS) and 1% penicillin/streptomycin (Sigma-Aldrich, Catalog#: P4333) at 37 ℃, humid atmosphere and 5% CO2. MDA-MB-468 and MAD-MB-231 were cultured in RPIM medium supplement 10% FBS and 1% penicillin/streptomycin.

METHOD DETAILS

Cell culture

The HEK293 $GnTI^-$ suspension cells were cultured using Gibco Freestyle 293 expression medium, which was supplemented with 1% fetal bovine serum and 1% non-essential amino acids from Gibco and infected with $GABRP_{\Delta}$ expressed virus. Transfected cells were harvested after 72 hours transfection. HEK293 cells were cultured using DMEM medium that was supplemented with 1% fetal bovine serum and 1% penicillin/streptomycin. HEK293 expressing $GABA_AR$ $\alpha1\beta2\gamma2$ (long form) are from Millipore Sigma and cultured in DMEM medium that was supplemented with 1% fetal bovine serum and 1% penicillin/streptomycin. MDA-MB-468 and MAD-MB-231 were cultured in RPIM medium supplement 10% FBS and 1% penicillin/streptomycin.

Construct description

The full-length human GABRP gene (Gene ID 2568) was obtained from Sino Biotechnology. To create the $GABRP_{\Delta}$ construct, a segment of the M3/M4 cytoplasmic loop spanning from Gln333 to Ser412 was replaced with an SQPARAA linker,[23,51] and a twin-Strep tag was attached to the C terminus. The resulting $GABRP_{\Delta}$ gene was then inserted into the pEZT BacMam vector.[52] The full-length GABRP gene and $GABRP_{\Delta}$ gene were also cloned into pLenti-C-Myc-DDK-IRES-Puro Vector for GABRP and $GABRP_{\Delta}$ stable cell lines construction. The corrected plasmid was confirmed by sequencing and used for the further experiments. The lentivirus for making stable cell lines which express full-length GABRP and $GABRP_{\Delta}$ were generated based on the standard protocol. HEK293 cell were infected with the virus and selected with 1μg/ml puromycin. The stable cell lines which can express GABRP and $GABRP_{\Delta}$ were validated with western blot.

Expression and purification of human $GABRP_{\Delta}$

To generate Bac-Mam P1 virus for $GABRP_{\Delta}$ expression, standard procedures were followed, and the resulting virus was amplified to obtain P2 virus. The virus titer was determined by expressing a small amount of $GABRP_{\Delta}$ in HEK293 $GnTI^-$ suspension cells.[53,54] Expression of $GABRP_{\Delta}$ was achieved by infecting HEK293 $GnTI^-$ suspension cells at a density of 2.5-3 × 10^6 cells/ml with the virus, and then adding valproic acid (Sigma-Aldrich) to a concentration of 5 mM to boost protein expression after 24 hours post-infection. The infected cells were then harvested after 72 hours post-infection by centrifugation and washed one time with HBS buffer (20 mM HEPES pH 7.4, 150 mM NaCl). For protein purification, cell pellet was resuspended in HBS buffer containing 1% (v/v) mammalian protease inhibitor cocktail (Sigma-Aldrich). The cells were sonicated for 5 min for 5 cycles, and cell debris was removed by centrifugation at 8,000 rpm for 30 min. This was followed by centrifugation at 100,000 g for 1 hour to pellet the cell membranes. Membrane pellets were mechanically homogenized and solubilized in HBS buffer containing 2% SMALP 200 (Cube Biotech) and 1% mammalian protease inhibitor cocktail for 12 hours at 4℃ with gentle shaking. The solubilized membranes were then centrifuged at 100,000 g for 1 hour to collect the supernatant. Then, the supernatant was mixed with Strep-Tactin XT Superflow affinity resins (IBA-Lifesciences) that had been equilibrated with HBS. The resulting slurry was allowed to shake gently for 1 hour at 4℃. The resin was then washed with HBS buffer and protein eluted using the same buffer containing 10 mM biotin (IBA-Lifesciences). The eluted sample was collected and used for the further experiments.

Cryo-EM sample preparation

Purified $GABRP_{\Delta}$ was concentrated using ultrafiltration and loaded onto a Superdex 200 increase 10/300 GL column equilibrated with HBS buffer. The peak fraction was then concentrated to 2 mg/ml. For cryo-electron microscopy, 3 μl of purified $GABRP_{\Delta}$ with or without 5 mM GABA were applied onto glow-discharged gold R1.2/1.3 300 mesh ultraAuFoil grids (Quantifoil) and immediately blotted for 8 s at 100% humidity and 16℃. The grids were then plunge-frozen into liquid ethane cooled by liquid nitrogen using a Vitrobot Mark IV (FEI).

Cryo-EM image collection and processing

Electron microscopy images were acquired at the Laboratory of Biomolecular Structure (LBMS) at Brookhaven National Laboratory (BNL) using a Titan Krios electron microscope (FEI) operated at 300 keV. The images were collected using a K3 summit direct electron detector (Gatan) equipped with a GIF quantum energy filter (15 eV) in super-resolution mode, with a super-resolution pixel size of 0.825 Å/pixel. A total of 6,500 images were collected over two 48 h sessions, with each micrograph exposed for 2.3 seconds and a total dose of 50 e/$Å^2$, 40 frames per micrograph. The images were recorded using the automated acquisition program EPU (FEI) with defocus values ranging from -0.8 μm to -2 μm. For sample-specific data collection parameters, please refer to Table S1.

The datasets were analyzed using a standardized processing pipeline in cryoSPARC.[47] Initially, motion-correction and contrast transfer function estimation were performed on all images. Poor-quality images were manually discarded after inspection. Next, a small set of images was manually used for particle picking, followed by 2D classification. The selected 2D classes were then

used as templates for automated particle picking from all images. Several rounds of 2D classification were performed for all particles, and the well-aligned 2D classes that showed clear 3D projections of $GABA_A$ receptors were chosen for 3D reconstruction. *Ab initio* model reconstruction was used to generate initial 3D models. Particles corresponding to different classes were selected and optimized through iterative rounds of heterogeneous refinement in cryoSPARC. The best models were refined using homogeneous and non-uniform refinement, and the overall resolutions of the final models were calculated using the Fourier shell correlation (FSC) at 0.143 cutoff. A local resolution map was generated with the program in cryoSPARC, based on the resolution range determined by the FSC output from the final non-uniform refinement. Finally, the maps were colored by local resolution estimation by opening the main 3D map and the local resolution map in UCSF ChimeraX[50] and analyzing them using the surface color tool.

Model building, refinement, validation

Software used in this project was curated by SBGrid.[55] The model building process was conducted in ChimeraX,[50] utilizing the PDB file generated from AlphaFold[56,57] as template. The initial GABRP pentamer model was generated by rigid body fitting the subunit models to the density map. A high-quality model was achieved through multiple rounds of iterative model building and refinement using Coot[48] and Phenix.[49] Detailed parameters and statistics for the model building and refinement process are provided in Table S1.

Whole-cell recordings in HEK293

Cells expressing GABA receptor were recorded after plating on poly-L-lysine coated 35 mm dishes for 24 h. The patch electrodes were pulled from 1.5-mm OD borosilicate capillary glass (World Precision Instruments). Electrodes had a resistance of 3-4 megohms. The bath solution is composed of: 140 mM NaCl, 4.7 mM KCl, 1.2 mM $MgCl_2$, 2.52 mM $CaCl_2$, 11 mM glucose and 5 mM HEPES (pH 7.4). Internal solution containing: 140 mM KCl, 1 mM $MgCl_2$, 11 mM EGTA, 10 mM HEPES, 1 mM $CaCl_2$, 2 mM K_2-ATP (pH 7.2). Inward currents were recorded with an EPC7 amplifier (HEK) using whole cell configuration of the patch-clamp technique. HEK cells were clamped at -60 mV. Recordings were carried out at room temperature (20 - 22℃). Series resistance was 2-4 megohms and was compensated by 80%–85%. Data were acquired at 10 kHZ and filtered at 5 kHZ using pCLAMP9 software (Molecular Devices). For qualitative experiments: Brief application of agonist was carried out by applying pressure pulses (1 s) to a GABA-containing glass pipette (tip diameter 1 mm, 1 M GABA), positioned ~100 μm from the cell. For quantitative experiments: Different concentrations of GABA in external solution were superfused over each recorded cell using a multichannel pipette (Computer-controlled Valve Control System from Warner Instruments) that switched the superfusing solution in < 1 millisecond.

C11 antibody generation

To generate an antibody specifically targeting GABRP, the purified GABRP ECD protein was used as an antigen to perform biopan screening from a phage display Fab (fragment antigen-binding) library.[58,59]GABRP ECD encoding gene was cloned into the pVRC vector with C-terminal Fc (fragment crystallizable region) fusion. GABRP ECD-Fc was expressed in Expi293 cells according to the manufacturer's protocol (Gibco, A14635). After 96 hours of transfection, the medium was collected by centrifugation at 6,000 rpm for 15 minutes. The medium was then filtered through a 0.45 μm PVDF filter and applied to protein A agarose (GE Healthcare). Protein A beads were washed with 50 column volumes of PBS buffer and eluted with elution buffer (50 mM NaH2PO4, 100 mM H3PO4, 140 mM NaCl, pH 2.8), which was subsequently neutralized with 1 M Tris-HCl pH 11.0. The eluted proteins were injected into a 10/300 Superdex 200 increase column that was equilibrated with 20 mM HEPES pH 7.5, 100 mM NaCl for further purification. Fractions corresponding to GABRP ECD-Fc were combined and concentrated using an ultracentrifuge tube with a molecular weight cut-off of 30 kDa. The concentrated protein was then incubated with FactorX (NEB) protease overnight at 4°C, and GABRP ECD was purified by collecting the flowthrough after incubating Factor Xa-treated samples with protein A agarose.

The phage-displayed synthetic antibody library F[59] was used to create phage pools, which were subjected to five rounds of selection using GABRP ECD immobilized on 96-well MaxiSorp immunoplates as the antigen, as previously described. After rounds four and five, culture supernatants from 96 clones were grown in 96-well deep well plates and used directly in phage ELISAs to identify clones specifically binding to GABRP ECD. GABRP-specific clones were then subjected to DNA sequence analysis.

For the recombinant humanized monoclonal C11-IgG production, the cDNAs encoding variable regions of heavy ang light chains of Fab C11 were cloned into the expression plasmids containing the human IgG1 heavy chain and Ig kappa light chain constant regions (InvivoGen), respectively. The recombinant antibodies were produced in Expi293 cells flowing the transfection with both the IgG1 heavy and light chain expression plasmids according to the protocols from Gibco (Gibco, A14635). The antibodies were purified from cell culture supernatants using Protein-A affinity chromatography with the same protocols as Fab purification as described perilously.

MAPK/ERK activation evaluation

To assess the activation of the MAPK/ERK, $GABRP_\Delta$ and GABRP overexpressed stable cells were seeded on to six well plates (Corning) coated with poly-D-lysine at 2.5×10^5 cells/well. After 24 h, the medium was replaced with serum-free medium. After 16 hours starvation, the cells were stimulated with different concentrations of GABA (0, 1, 10, 100, 1000, 10000 μM), or muscimol (10000 μM) or baclofen (10000 μM) for 5 min at 37 °C followed by washing with ice cold PBS, harvested in RIPA lysis buffer containing 50 mM Tris (pH 7.4), 150 mM NaCl, 0.5 % NaDC, 0.1 % SDS, 1 % NP-40, 1% (v/v) mammalian protease inhibitor cocktail (Sigma-Aldrich). For

antagonist inhibition assays, the starved cells were pretreated with Picrotoxin (PTX-A), Gallein or C11 IgG for 1 hour or Pertussis Toxin (PTX-B) for 12 hours and then stimulated with GABA followed the previous protocol. Samples were centrifuged and the supernatants were prepared for SDS-PAGE. After electrophoresis, proteins were transferred to PVDF membranes for Phosho-Erk1/2 and total Erk1/2 detection. The Phosho-Erk1/2(Thr^{202}/Tyr^{204}) and Erk1/2 antibodies were from Cell Signaling Technology. The bands for phosho-Erk1/2 (Thr^{202}/Tyr^{204}) and total Erk1/2 proteins were quantified using ImageJ 1.51 h. The relative ratios for p-Erk/Erk were plotted with Graphpad Prism 9.4.0.

Characterization of the cytotoxic effect of inhibitors on breast cancer cell lines

To evaluate the *in vitro* growth inhibitory effects of inhibitors, we cultured MDA-MB-468 and MDA-MB-231 breast cancer cells with RPIM1640 plus 10%FBS. Cells were seeded at 5000 cells per well (triplicates for each dilution group) in 96-well plates and allowed to attach overnight. Cells were then exposed with C11-IgG (100 nM), Gallein (10 μM) or AS-041164 (10 μM) for 72 hours. Viable cell were measured in each well using the ATP-based CellTiter-Glo® luminescent cell-viability assay (Promega).

Data-independent mass spectrometry based phosphoproteomics

GABRP$_{\Delta}$ stable cells in response to GABA (1 mM) were measured in five biological replicates. The cell lysis was performed with 10 M urea buffer containing protease and phosphatase inhibitors (cOmplete™, Roche and Halt™, Thermo Scientific) and ultrasonically lysed by VialTweeter (Hielscher-Ultrasound Technology).[60,61] A total of 700 μg proteins per replicate were processed and digested by sequencing grade porcine trypsin (Promega) at a ratio of 1:20 overnight at 37 °C, as described previously.[60] Then, 250 μg of purified peptides per sample were used for the phosphopeptide enrichment using High-Select™ Fe-NTA kit (Thermo Scientific, #A32992) according to vendor instruction. All phosphoproteomics samples were respectively measured by a 150-min DIA mass spectrometry (DIA-MS) method on the Orbitrap Fusion Lumos Tribrid mass spectrometer (Thermo Scientific).[34,61] The DIA-MS method consisted of one MS1 full scan and 33 MS2 scans of variable windows. The MS1 scan range was 350 – 1650 m/z and the MS1 resolution was 120,000 at m/z 200. The MS1 full scan AGC target value was set to be 2.0E6 and the maximum injection time was 50 ms. The MS2 resolution was set to be 30,000 with the scan range 200 – 1800 m/z. The normalized HCD collision energy was 28%. The MS2 AGC was set to be 1.5E6 and the maximum injection time was 50 ms. As for phosphoproteomic data processing, all the raw data were searched on Spectronaut v18 (Biognosys AG, Switzerland) with directDIA algorithm[62] during which Phosphorylation at serine/threonine/tyrosine (S/T/Y) were set as variable modifications. The PTM localization score was kept >0.75 on the global experimental level while the quantitative data at the phosphopeptide precursor level were reported using PTM score 0.01, as described.[34,61] Both peptide and protein FDR (Qvalue) were controlled below 1%. All the other settings in Spectronaut were kept as Default. The mass spectrometry raw dataset has been deposited to the ProteomeXchange Consortium via the PRIDE partner repository[63] with the dataset identifier PXD044482.

QUANTIFICATION AND STATISTICAL ANALYSIS

Overall and local resolution values for cryo-EM maps (Figure S2) were calculated using Cryosparc, based on the gold-standard Fourier Shell Correlation (GFSC) method with 0.143 criterion. Refinement statistics in the Table S1 for the atomic coordinates were calculated using Phenix. Biological replicates are noted in the relevant legends.